

Pt–Au/C cathode with enhanced oxygen-reduction activity in PEFCs

G SELVARANI, S VINOD SELVAGANESH, P SRIDHAR*, S PITCHUMANI and A K SHUKLA†

CSIR-Central Electrochemical Research Institute-Madras Unit, CSIR Madras Complex, Chennai 600 113, India

†Solid State and Structural Chemistry Unit, Indian Institute of Science, Bangalore 560 012, India

MS received 27 September 2010; revised 20 December 2010

Abstract. Carbon-supported Pt–Au (Pt–Au/C) catalyst is prepared separately by impregnation, colloidal and micro-emulsion methods, and characterized by physical and electrochemical methods. Highest catalytic activity towards oxygen-reduction reaction (ORR) is exhibited by Pt–Au/C catalyst prepared by colloidal method. The optimum atomic ratio of Pt to Au in Pt–Au/C catalyst prepared by colloidal method is determined using linear-sweep and cyclic voltammetry in conjunction with cell-polarization studies. Among 3:1, 2:1 and 1:1 Pt–Au/C catalysts, (3:1) Pt–Au/C exhibits maximum electrochemical activity towards ORR. Powder X-ray diffraction pattern and transmission electron micrograph suggest Pt–Au alloy nanoparticles to be well dispersed onto the carbon-support. Energy dispersive X-ray analysis and inductively coupled plasma-optical emission spectroscopy data suggest that the atomic ratios of the alloying elements match well with the expected values. A polymer electrolyte fuel cell (PEFC) operating at 0.6 V with (3:1) Pt–Au/C cathode delivers a maximum power-density of 0.65 W/cm² in relation to 0.53 W/cm² delivered by the PEFC with pristine carbon-supported Pt cathode.

Keywords. Polymer electrolyte fuel cells; cathode catalyst; platinum–gold alloy; oxygen-reduction reaction.

1. Introduction

Polymer electrolyte fuel cells (PEFCs) are being perceived as promising alternative power source for various mobile and stationary power applications due to their high efficiency, quick start-up and low operating-temperature. However, the extent of oxygen-reduction kinetics at cathode in PEFCs happens to be several orders lower than the hydrogen-oxidation kinetics at the anode, which leads to a higher over-potential at the cathode and to consequent reduction in performance and efficiency of the PEFCs (Bockris and Srinivasan 1969; Gottesfeld and Zawodzinski 1997). Accordingly, a PEFC cathode-electrocatalyst that can ameliorate oxygen-reduction reaction (ORR) is much desired for PEFCs.

Owing to the acidic nature of polymer-membrane electrolyte and low-temperature operation of PEFCs, the use of non-noble catalysts has met only a limited success (Fernandez *et al* 2005; Shao *et al* 2006a, b). At present, platinum (Pt) is widely used as a catalyst in PEFCs, due to its high activity towards ORR. However, Pt is expensive and its resources are limited. Furthermore, the activity of Pt towards ORR remains much lower than is desired due to high activation-overvoltage (Gasteiger *et al* 2005). In the literature (Antolini *et al* 2005; Lima *et al* 2006; Yuan *et al* 2006; Gong *et al* 2007), addition of base metals, such as iron, cobalt, nickel, chromium, to Pt is known to ameliorate ORR. However, the resulting Pt-base metal alloy catalysts exhibit poor long-term stability due to the dissolution of transition metal (Pourbaix 1974).

Accordingly, efforts are being made to find a long-lasting and active catalyst for PEFCs. In this context, introduction of second noble metal, such as palladium, gold, to Pt has received considerable attention in recent years due to their attractive stability and activity towards ORR in fuel cells (Li *et al* 2004; Shao *et al* 2006a, b; Hernandez-Fernandez *et al* 2007; Mathiyarasu and Phani 2007). Among the various noble metals, gold is of particular interest in view of its inertness in the bulk state but high catalytic activity at nano-scales. Janssens *et al* (2006) reported a dramatic increase in the catalytic activity with gold particles <5 nm which has also been corroborated by El-Deab and Osaka (2002a, b, 2003).

Pristine Au as electrocatalyst has been intensively investigated for fuel cell applications and different methods of preparation for Au nanoparticles and their performance towards ORR have been reported in the literature (Haruta 1997; Berg *et al* 1998; El-Deab and Osaka 2002a, b; Xu and Mavrikakis 2003). The electrocatalytic behaviour of Au nanoparticles is attributed to an enrichment of the step orientation of the Au surface that is considered to be an active reaction-site for ORR (El-Deab and Osaka 2002a, b). However, the electrocatalytic activity of Au still stands lower than Pt. Accordingly, it is not feasible to replace Pt with pristine Au as electrocatalyst.

Generally, the rate-determining step for ORR is the splitting of the O=O bond to form water. The kinetics of reaction depends on the degree of interaction of oxygen with catalyst-adsorption sites. The guidelines for designing bimetallic catalysts suggest that one of the metals in the bimetal catalyst should facilitate the splitting of O=O bond while the

*Author for correspondence (psridhar55@gmail.com)

other should help reduce the adsorbed atomic-oxygen (Luo *et al* 2006). In this context, the combination of Pt and Au has been found to be superior to pristine Pt towards ORR (Elhissen *et al* 1999; Devarajan *et al* 2005; Luo *et al* 2005; Njoki *et al* 2005; Qian *et al* 2006; Hernandez-Fernandez *et al* 2008; Wang *et al* 2008, 2009; Liu *et al* 2009a, b; Ma *et al* 2010). In view of the unique properties of nano-sized gold (Haruta 2005; Hughes *et al* 2005; Luo *et al* 2006) and the high catalytic-activity of Pt, bimetallic Pt–Au nanoparticles of optimum composition are highly likely to serve as synergistic catalysts. It is also reported that the intra-alloy charge transfer from Pt to Au in the Pt–Au alloy catalyst increases the extent of *d*-orbital vacancy in Pt (Goodenough *et al* 1989; Berg *et al* 1998). Accordingly, Pt–Au nanoparticle is expected to be synergistic to ORR at the PEFC cathode. In the literature, silica-supported Pt–Au nanoparticles have been studied intensively (Luo *et al* 2006; Mott *et al* 2007). Several authors (Hernandez-Fernandez *et al* 2007, 2008; Wang *et al* 2008, 2009; Liu *et al* 2009a, b; Ma *et al* 2010) have reported the influence of catalyst preparation of bimetallic Pt–Au nanoparticles on ORR. Although high activity of Pt–Au catalyst towards ORR is claimed, its performance in fuel cells remains limited and the effect of varying Pt to Au ratio in the Pt–Au alloy catalyst on ORR remains unexplored.

In the present study, Pt–Au/C catalyst is prepared separately by impregnation, colloidal and micro-emulsion methods and the optimum catalyst composition is established by linear-sweep voltammetry (LSV) in conjunction with cell-polarization studies. The extent of alloy formation, mean particle-size and morphology of Pt–Au/C are studied by powder X-ray diffraction (XRD) and transmission electron microscopy (TEM). The bulk and surface compositions of Pt and Au in Pt–Au/C catalysts are determined using inductively-coupled-plasma optical emission spectroscopy (ICP-OES) and energy-dispersive analysis by X-rays (EDAX), respectively.

2. Experimental

2.1 Preparation of carbon-supported Pt–Au catalyst

To prepare Pt–Au/C by the impregnation method, the required amounts of the metal precursors, viz. H_2PtCl_6 and HAuCl_4 , were dissolved in a solution containing water and 2-propanol, and pH of the solution was adjusted to ~ 4 by adding Na_2CO_3 . The resulting mixture was added drop wise to a dispersion of carbon (Vulcan XC72R) in water under reflux. Subsequently, alkali-stabilized sodium borohydride was added to the mixture and stirred continuously for 3 h. Pt–Au/C catalyst was obtained after filtering and washing with distilled water followed by drying overnight in an air oven at 80°C .

In the colloidal method, the required amount of hydrogen tetrachloroaurate (HAuCl_4) solution was added drop-by-drop at 40°C to a platinum–metal precursor, viz.

$\text{Na}_2[\text{Pt}(\text{SO}_3)_4]$, dissolved in acidified water, followed by drop-wise addition of 15 w/o hydrogen peroxide with continuous stirring at 60°C that resulted in vigorous gas evolution. The solution was further stirred for 1 h. Subsequently, the required amount of carbon slurry was added to it. Finally, Pt–Au/C was obtained by passing hydrogen gas for 2 h at 80°C that was filtered, washed copiously with hot distilled-water, and dried overnight in an air oven at 80°C .

In the micro-emulsion method, the required amount of metal precursor viz. H_2PtCl_6 and HAuCl_4 , carbon and hydrazine were dissolved separately in micro-emulsion containing sodium *bis* (2-ethylhexyl sulfosuccinate), water and isooctane. Then, micro emulsion containing the metal precursors was slowly added to micro-emulsion of carbon with constant stirring followed by the addition of micro-emulsion containing excess of hydrazine with continued stirring overnight. Pt–Au/C was obtained by the addition of tetrahydrofuran that was washed with water/ethanol mixture to remove excess surfactant followed by drying overnight at 80°C .

2.2 Electrochemical characterization

2.2a Half-cell studies: To study the activity of Pt/C and Pt–Au/C catalysts, LSV and CV measurements were performed using a computer-controlled electrochemical analyser (Autolab PGSTAT-30). For LSV experiments, the electrode rotation speeds were controlled by EcoChemie RDE – 70296 Unit. Glassy carbon (GC) disk was used as the working-electrode substrate in the study. Prior to each experiment, the electrode was polished with $0.06\ \mu\text{m}$ alumina to obtain a mirror-finished surface followed by rinsing with distilled water in an ultrasonic bath. To prepare the working electrode, catalyst (Pt/C or Pt–Au/C) suspension was obtained by adding catalyst to water followed by Nafion ionomer addition and sonication for 30 min. The suspension was quantitatively transferred to the surface of polished GC disk. The electrode was dried at room temperature ($\sim 25^\circ\text{C}$). A saturated calomel electrode (SCE) and a Pt foil were used as reference and counter electrodes, respectively in the 3-electrode-cell configuration.

In order to clean and activate the working electrode, it was cycled between $-0.25\ \text{V}$ and $0.8\ \text{V}$ with respect to SCE at a sweep rate of $50\ \text{mV/s}$ in de-aerated ($0.5\ \text{M}\ \text{H}_2\text{SO}_4$) electrolyte until stable and reproducible voltammograms were obtained. The cyclic voltammograms were recorded once the working electrode was well equilibrated. LSV experiments were performed using RDE in oxygen saturated aqueous $0.5\ \text{M}\ \text{H}_2\text{SO}_4$. The concentration of the dissolved oxygen in saturated aqueous $0.5\ \text{M}\ \text{H}_2\text{SO}_4$ being $\sim 1\ \text{mM}$ (Lide 1995). LSV data were recorded in the cathodic-sweep direction at $3\ \text{mV/s}$ between $0.8\ \text{V}$ and $0\ \text{V}$ vs SCE with varying rotations ($400\text{--}2400\ \text{rpm}$) at room temperature.

2.2b Fuel-cell studies: Fabrication of membrane electrode assemblies (MEAs): MEAs were fabricated as reported

elsewhere (Selvarani *et al* 2009a, b). In brief, both anode and cathode contained a backing layer, a gas-diffusion layer and a catalyst layer. A teflonized (15 w/o) carbon paper (Toray-TGP-H-120) of 0.35 mm thickness was employed as the backing layer to these electrodes. To prepare the gas-diffusion layer, carbon was suspended in cyclohexane and agitated in an ultrasonic water bath for 30 min. To this mixture, 15 w/o Teflon suspension was added under sonication. The resultant slurry was coated onto a teflonized carbon paper followed by sintering at 350 °C for 30 min.

To prepare the catalyst layer, required amount of Pt/C or Pt–Au/C was suspended in isopropyl alcohol. The mixture was agitated in an ultrasonic water bath, and 7 and 30 w/o of Nafion (Dupont) dispersion was added to anode and cathode slurries, respectively with continuing ultrasonication for 30 min. The resulting ink was coated on a gas-diffusion layer. Both anode and cathode contained a platinum loading of 0.5 mg cm⁻² (active area, 25 cm²) which was kept identical in all the MEAs. To establish effective contact between the catalyst layer and the polymer electrolyte, a thin layer of Nafion ionomer (5 w/o) diluted with isopropyl alcohol in 1:1 ratio was spread onto the surface of each electrode. MEAs were obtained by hot pressing the cathode and anode on either side of a pretreated-Nafion 1135 membrane under a compaction pressure of 60 kg cm⁻² at 130°C for 3 min.

2.2c Cell-polarization studies: MEAs were evaluated using a conventional 25 cm² fuel-cell fixture with parallel serpentine-flow-field machined on graphite plates obtained from M/s Schunk Kohlenstofftechnik GmbH, Germany. After equilibration, galvanostatic-polarization data for the cells were obtained at 60°C at varying load current-densities with humidified hydrogen and oxygen feeds at atmospheric pressure at anode and cathode, respectively, using a LCN100-36 electronic load procured from Bitrode Corporation, US.

2.3 Physical characterization

Powder XRD patterns for the catalysts were obtained on a Philips X'Pert Diffractometer using Cu K_α radiation ($\lambda = 1.5406 \text{ \AA}$) between 20° and 80° in reflection geometry in steps of 0.034°/min. The morphology of the catalysts was examined under a TCNAI 20 G2 transmission electron microscope (200 kV) by suspending catalyst particles in isopropyl alcohol and casting the sample by dropping the catalyst solution onto a carbon-coated copper grid followed by solvent evaporation in vacuum at room temperature.

The surface atomic compositions for Pt–Au/C catalysts with varying atomic ratios of Pt to Au were obtained with the help of a JEOL JSM 5400 scanning electron microscope coupled with energy dispersive X-ray analysis facility. For this study, the sample was prepared by pressing the catalyst powder onto a conducting carbon-tape pasted onto a copper stub.

ICP-OES was used to analyse the bulk composition of Pt and Au in Pt–Au/C catalysts with varying atomic ratios. For this purpose, the catalysts were dissolved in concentrated aqua regia, and subsequently diluted to concentrations ranging between 1 and 50 ppm as desired for the analysis. The actual composition was determined from the calibration curves for the known standards.

In the following text, Pt–Au/C catalyst prepared by impregnation, colloidal and micro-emulsion methods is represented as S-1, S-2 and S-3, respectively along with their atomic ratios as (1:1), (2:1) and (3:1). For example, Pt–Au/C catalyst prepared by colloidal method with atomic ratio 2:1 is represented as S-2(2:1) and the carbon-supported Pt catalyst (Pt/C) is represented as S-4.

3. Results and discussion

Pt–Au catalyst can be prepared both by chemical and electrochemical routes. But the former is more suitable for bulk preparation. In order to identify the most suitable chemical preparatory-route among impregnation, colloidal and micro-emulsion methods for Pt–Au catalyst, Pt–Au (2:1) composition is arbitrarily chosen and powder-XRD patterns for S-1 (2:1), S-2 (2:1) and S-3 (2:1) samples obtained, and compared with the powder XRD pattern for S-4 as shown in figure 1. The XRD pattern for S-2(2:1), S-3(2:1) and S-4 show characteristic peaks of face centred cubic (*fcc*) crystalline Pt at (111), (200), (220), and (311) reflections. The XRD peak corresponding to (111) plane for Pt in S-4 is observed at 39.7° and for pure Au at 38.2° (Selvarani *et al* 2009a); Pt (111) reflections for S-2(2:1) and S-3(2:1) catalysts are observed at 38.7° and 38.8°, respectively. The negative shift in (111) reflection for S-2(2:1) and S-3(2:1)

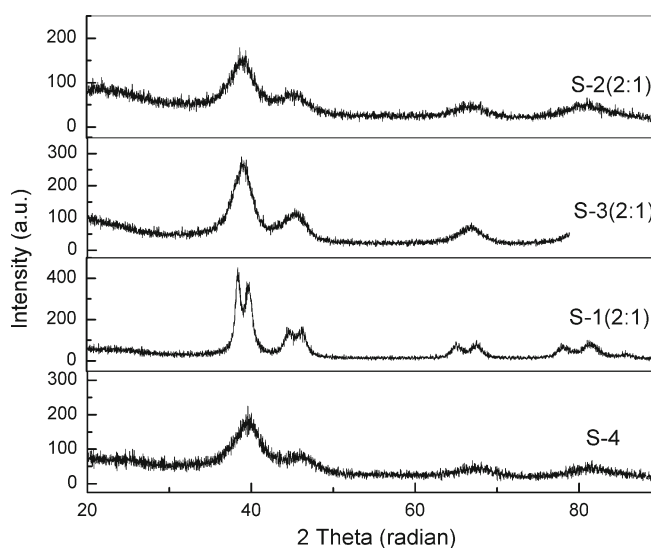


Figure 1. XRD patterns for (S-4) and S-1(2:1), S-2(2:1) and S-3(2:1) catalysts.

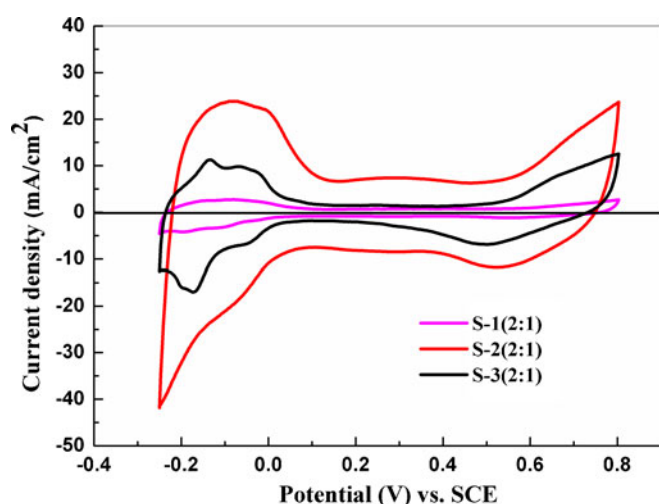


Figure 2. Steady-state cyclic voltammograms for S-1(2:1), S-2(2:1) and S-3(2:1) catalysts in N_2 -saturated 0.5 M H_2SO_4 .

catalysts in relation to S-4 confirms the alloy formation in Pt–Au catalysts. By contrast, the presence of (111) reflection at 38.2° for Au and 39.6° for Pt suggests the presence of Au and Pt as a physical mixture in S-1(2:1) catalyst. According to the binary phase-diagram, there is a miscibility gap between Pt and Au, and hence, phase segregation can be expected. Accordingly, appropriate thermal-treatment for the sample is required to obtain Pt–Au alloy (Bond 2007).

According to Bond (2007) although Pt–Au phase diagram shows a wide-miscibility gap due to limited solubility of the components, nano-sized particles form homogeneous alloys as all atoms retain their electronic structure, and re-hybridization due to band formation is hindered. Hence, a proper synthetic route is desirable for realizing bimetallic Pt–Au nanoparticles. In the literature, Pt and Au are reported to be present as individual elements in Pt–Au when colloidal method is used for its preparation (Hernandez-Fernandez *et al* 2007) while, in the present study, solid solutions of Pt–Au alloy are obtained by this method, which could be attributed to the precursor and reaction pH conditions. In the present study, the catalyst S-1(2:1) prepared by impregnation method yields segregated Pt and Au particles because the reduction of Au-ion proceeds faster than Pt-ion. In the

literature, it is reported that the catalyst prepared by impregnation method needs to be heated above $500^\circ C$ in order to obtain alloy while, in the present study, the heat treatment is avoided to preclude the formation of larger particles. In the light of the foregoing, a judicious selection of preparatory conditions, viz. precursor, solution pH, heating rate and the reaction temperature, is mandatory for synthesizing finely-divided Pt–Au alloy.

As a surface sensitive technique, CV detects the electrochemical properties of surface atoms rather than the bulk atoms (Kristian and Wang 2008). In addition, CV is a useful technique to analyse the influence of the particle size of catalyst on electrochemical surface-area (ESA). Steady-state cyclic voltammograms are shown for S-1(2:1), S-2(2:1) and S-3(2:1) catalysts in de-aerated 0.5M H_2SO_4 as shown in figure 2. All catalysts display features of hydrogen adsorption–desorption between -0.24 V and 0.1 V vs SCE followed by the “double-layer” region indicative of the presence of Pt component dominating on the surface of the bimetallic catalyst. During the anodic sweep, at potentials >0.45 V vs SCE, oxide film formation followed by its removal during the cathodic sweep is observed. The hydrogen adsorption/desorption charge (Q_H) for the S-1(2:1) catalyst is lower than that for S-2(2:1) and S-3(2:1) catalysts suggesting the ESA to be lower for S-1(2:1), which is attributed to the larger particles of the catalyst sample in relation to the other two catalysts. The values of Q_H and ESA for all the three catalysts are presented in table 1. From the powder-XRD patterns, it is clear that the S-1(2:1) catalyst has segregated Pt and Au particles; the voltammogram obtained for the catalyst shows characteristic peaks for hydrogen adsorption/desorption, double-layer region followed by oxide formation and reduction on Pt.

In order to analyse the influence of preparation condition on electrochemical activity of Pt–Au catalyst towards ORR, LSV study is conducted using RDE in oxygen-saturated aqueous H_2SO_4 . LSV data are recorded cathodically at 3 mV/s scan rate between 0.8 V and 0 V vs SCE at 1200 rpm. Figure 3 shows the ORR data for the S-1(2:1), S-2(2:1) and S-3(2:1) catalysts and their electrode-kinetic parameters, viz. onset potential, kinetic current-density at 0.6 V vs SCE and mass activity, are given in table 1. It is seen from these data that the onset potential, kinetic current and mass activities increase as S-1(2:1) < S-3(2:1) < S-2(2:1). Thus, among the

Table 1. Electrokinetic parameters for carbon-supported Pt–Au catalyst with different methods of preparation.

Catalyst	Charge Q_H (mC)	ESA (m^2/g)	Onset potential (V vs SCE)	Kinetic current density @ 0.6 V vs SCE (mA/cm^2)	Mass activity @ 0.6 V vs SCE (mA/g)
S-1(2:1)	11.7	11.1	0.739	0.99	1980
S-2(2:1)	80.5	76.7	0.752	4.64	9280
S-3(2:1)	44.8	42.7	0.742	2.26	4520

three Pt–Au/C catalysts prepared through different chemical routes, S-2(2:1) catalyst shows enhanced-activity towards ORR.

To validate the performance of various Pt–Au catalysts in a typical PEFC system, steady-state polarization curves are obtained with a H₂O₂ PEFC employing Pt–Au/C prepared through various methods and the data are presented in figure 4. Among these, Pt–Au/C prepared through colloidal route, viz. S-2(2:1), exhibits highest activity in the entire polarization region as compared to S-1(2:1) and S-3(2:1). These data confirm well with LSV studies. PEFC cathode comprising S-2(2:1) operating at 0.6 V delivers a power-density of 0.63 W/cm² in relation to 0.52 W/cm² and 0.43 W/cm² obtained with PEFC cathodes employing S-3(2:1) and S-1(2:1), respectively.

The aforesaid studies clearly indicate that the S-2(2:1) catalyst shows enhanced electrochemical activity towards ORR

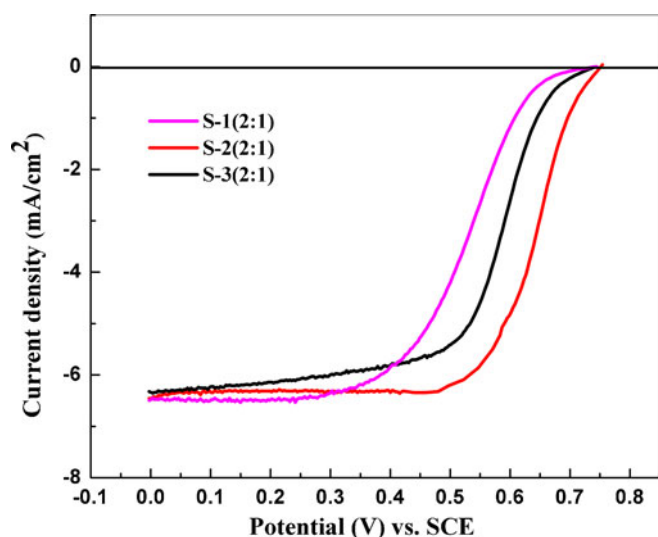


Figure 3. LSV measurements of S-1(2:1), S-2(2:1) and S-3(2:1) catalysts in O₂-saturated 0.5 M H₂SO₄ for ORR at 1200 rpm with a scan rate of 3 mV/s.

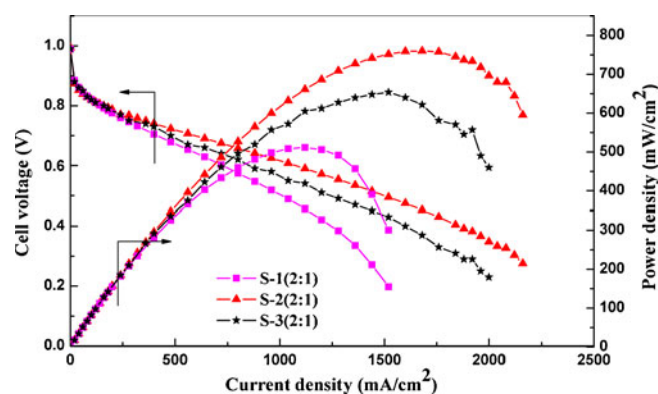


Figure 4. Steady-state performance of (H₂O₂) PEFC cathodes with S-1(2:1), S-2(2:1) and S-3(2:1).

in relation to S-1(2:1) and S-3(2:1). In order to obtain the maximum activity for ORR, S-2 catalyst with varying atomic compositions of Pt to Au, viz. 3:1 and 1:1, are prepared keeping the Pt content constant at 40 w/o. Carbon-supported 40 wt. % Pt (S-4) is also prepared by similar procedure for the sake of comparison.

Figure 5 shows TEM images for the S-2 catalyst with varying Pt to Au atomic ratios. It is seen that the Pt–Au alloy nanoparticles with a narrow particle-size distribution are well dispersed on the surface of the carbon-support. The mean size of the metal nanoparticles on carbon-support is obtained by measuring 200 randomly-chosen particles in the magnified TEM images (table 2). In S-2 (3:1), the catalyst particles have narrower size-distribution than S-2 (2:1) and S-2 (1:1). The mean particle-size for S-2 catalysts increases with increasing Au content. These values are in good agreement with XRD (data not shown for the sake of brevity) data and the particle-size measured from XRD data using Scherrer equation are presented in table 2. Although the XRD data for S-2(1:1) show nanometer-size particles, the TEM picture for S-2(1:1) shows ill-dispersed particles unlike other compositions. The high metal-to-support ratio in the catalyst is likely to induce such aggregation effects. Electron diffraction patterns for S-4 and S-2 catalysts with varying Pt to Au atomic ratio obtained from a selected area are presented in the inset of figure 5. The presence of a nano-sized alloy is evident through the ring pattern. However, S-2(1:1) alloy exhibits a broken ring due to clustered Pt–Au alloy particles.

Quantitative analysis of platinum to gold atomic ratio is performed by ICP-OES (table 2) which indicates the bulk composition of the Pt–Au alloy catalyst to be near the nominal value. Surface atomic compositions for the Pt–Au alloy catalysts are also obtained by EDAX analysis. EDAX spectra for S-2 catalyst with varying Pt to Au atomic ratios, viz. S-2(1:1), S-2(2:1) and S-2(3:1), are obtained and it is found that the composition on the surface of the catalysts are closer to the nominal values. The EDAX compositions obtained for all the alloy catalysts prepared during this study are presented in table 2. The data suggest that the surface compositions of the Pt–Au alloy catalysts are nearly similar to the bulk.

To analyse the electrochemical activity of S-2 with varying atomic ratios, a steady-state CV study is carried out in de-aerated 0.5M H₂SO₄ and data are presented in figure 6. In the cyclic voltammogram, all the catalysts display the features of Pt-characteristic region. The ESA derived from area under adsorption peaks are presented in table 3. Lower values of ESA for S-2 catalysts are attributed to larger particle size for Pt–Au than Pt/C (S-4). These values are in good agreement with TEM results.

To further examine the effect of composition of Pt to Au in S-2(2:1) catalyst towards ORR, LSV study is conducted using RDE at 1200 rpm in oxygen-saturated H₂SO₄ with a scan rate of 3 mV/s and compared with S-4 (figure 7). S-2(3:1) shows enhanced ORR activity in relation to S-2(2:1) and S-2(1:1), and all S-2 catalysts perform better than S-4. The electrode-kinetic parameters, viz. onset potential, kinetic

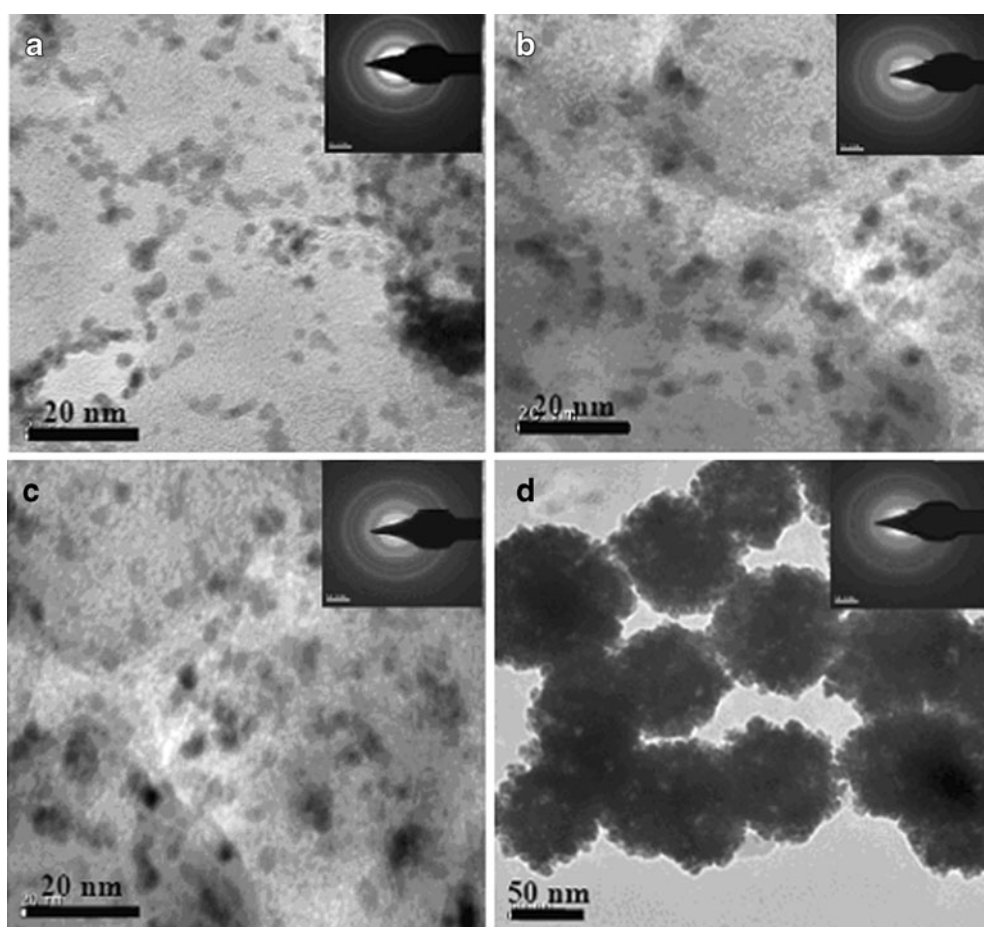


Figure 5. Transmission electron micrographs and electron diffraction patterns for **a.** S-4, **b.** S-2 (3:1), **c.** S-2 (2:1), and **d.** S-2 (1:1) catalysts.

current-density at 0.6 V vs SCE and mass activity are presented in table 3. It is found that the onset potentials, mass activity and kinetic current density vary as: S-2 (3:1) > S-2 (2:1) > S-2 (1:1) > S-4.

The catalysts have also been performance tested in PEFCs. The cell polarization data for S-2 with varying Pt to Au atomic ratio, viz. S-2(3:1), S-2(2:1) and S-2(1:1), in a H₂ / O₂ PEFC are compared with the PEFC employing S-4 catalyst electrodes and the data are presented in figure 8. PEFC cathodes employing S-2 with all the three atomic ratios perform

Table 2. Composition and structural parameters for S-4 and S-2 catalysts with varying atomic ratios.

Catalyst	Particle size,		Atomic ratio (ICP-OES) %	Atomic ratio (EDAX) %
	TEM (nm)	XRD (nm)		
S-2(3:1)	4.3	4.6	74.35: 25.65	71.65: 28.35
S-2(2:1)	4.5	4.9	65.8: 34.2	66.25: 33.75
S-2(1:1)	–	5.3	49.44: 50.55	50.31: 49.69
S-4	3.5	3.9	–	–

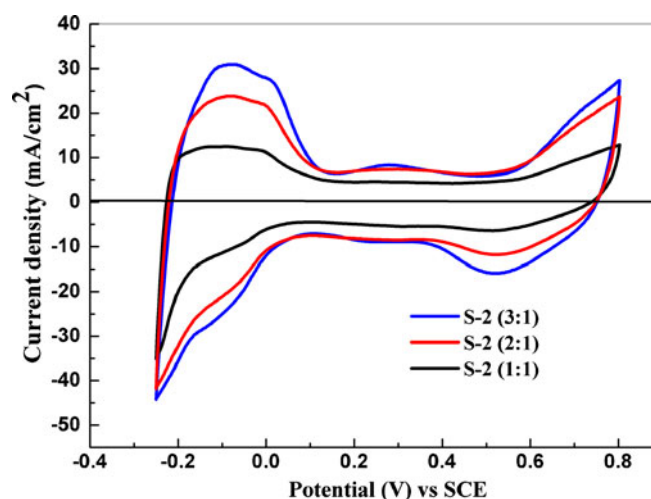


Figure 6. Steady-state cyclic voltammograms for S-2(3:1), S-2(2:1), and S-2(1:1) catalysts in N₂-saturated 0.5 M H₂SO₄.

better than the PEFC cathode with S-4. PEFC cathode comprising S-2(3:1) exhibits a power-density of 0.65 W/cm² at

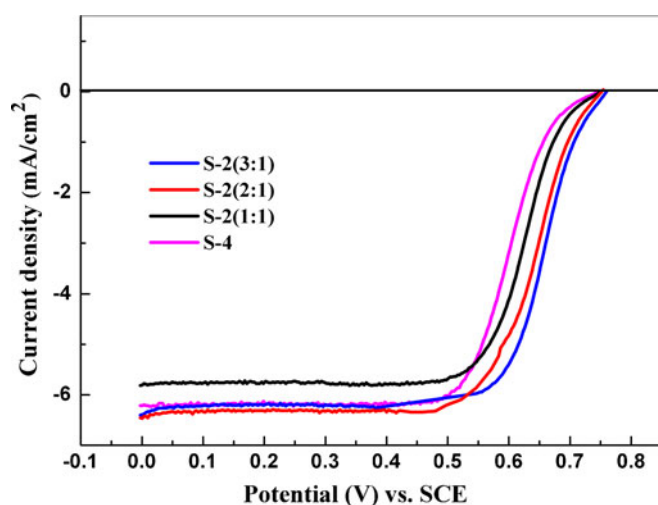
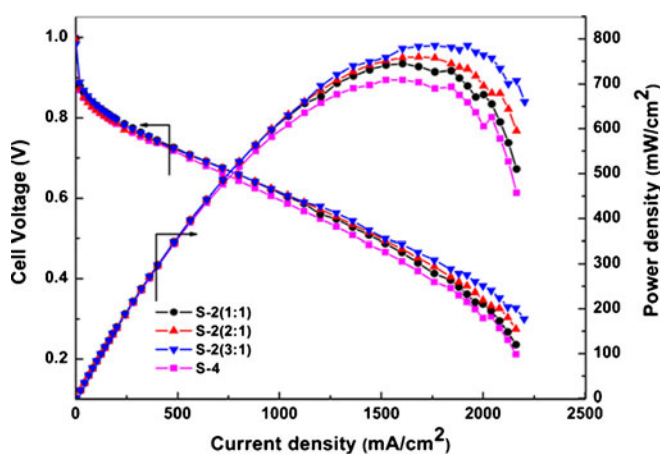
Table 3. Electrokinetic parameters for S-4 and S-2 catalysts with varying atomic ratios.

Catalyst	Charge Q_H (mC/cm ²)	ESA (m ² /g)	Onset potential (V vs SCE)	Kinetic current density @ 0.6 V vs SCE (mA/cm ²)	Mass activity @ 0.6 V vs SCE (mA/g)
S-2(3:1)	105.4	100.4	0.757	5.21	10420
S-2(2:1)	80.5	76.7	0.751	4.63	9260
S-2(1:1)	47.7	45.4	0.748	3.80	7720
S-4	120.6	114.8	0.745	2.81	5620

0.6 V in relation to 0.53 W/cm² at the same cell voltage delivered by the PEFC cathode with S-4. Since the anode, electrolyte, reactant and testing conditions in all the PEFCs are identical, the enhanced performance of the former is merely due to Pt–Au alloy catalyst. These data support CV and LSV data.

Generally, the rate-determining step for ORR is breaking of O–O bond to form water. The kinetics of the reaction depends on the degree of interaction of oxygen with catalyst adsorption sites. The enhanced electro-catalytic activity for Pt–Au alloy can be explained in the light of the electronic factor, viz. the change of the *d*-band vacancy in Pt upon alloying and/or by a geometric effect. These effects may enhance the reaction rate for oxygen adsorption and cleavage of O=O bond during the reduction reaction. The enhanced catalytic activity of Pt–Au alloy is also elucidated in an earlier study using X-ray photoelectron spectroscopy (Selvarani *et al* 2009a). Au 4 $f_{7/2}$ binding energy values for Au foil and Au in Pt–Au catalyst are found to be 83.88 eV and 83.50 eV, respectively. The shift in binding energy value suggests an intra-alloy charge transfer from Pt

to Au due to the higher electro-negativity of Au (2.54) in relation to Pt (2.2). The higher electro-negativity for Au in relation to Pt increases *d*-orbital vacancies in Pt metal, resulting in increased electro-catalytic activity towards ORR. Density functional theory (DFT) calculations reflect a distorted geometry for Pt–Au alloy catalyst in relation to pristine Pt and Au suggesting that Au atoms tend to occupy the corner positions (surface sites) in the presence of Pt (Selvarani *et al* 2009a). The orientation of Au atoms at surface sites with low coordination is attributed to (a) the relative cohesive energies, (b) electro-negativity values, and (c) electronic/steric effects. Data obtained from electronic parameters of modeled cluster indicate that the incorporation of Au to Pt matrix alters the distance of Pt–Pt and reduces the charge density on Pt. Furthermore, with increasing Au content in Pt–Au (3:1) in relation to Pt–Au (1:1), the charge density on Pt decreases. It is noteworthy that Au atoms with low coordination numbers have higher-lying *d* states more reactive and interact strongly with the adsorbate states (Lopez and Norskov 2002). In the light of the foregoing, S-2(1:1) is expected to be superior than S-2(3:1). But contrary to this, S-2(1:1) with higher Au content than S-2(3:1) experiences lack of active Pt-sites on its surface for promoting ORR, resulting in reduced catalytic

**Figure 7.** LSV measurements of S-4 and S-2 catalysts in O₂-saturated 0.5 M H₂SO₄ for ORR at 1200 rpm with a scan rate of 3 mV/s.**Figure 8.** Steady-state performance of (H₂–O₂) PEFCs with S-4 and S-2 cathode catalysts.

activity. These arguments favour the present experimental findings.

To further understand ORR on S-2(3:1) cathode catalyst, the electrode-kinetic parameters, viz. the number of electrons transferred during ORR and order of the reaction, have been obtained. ORR may either proceed through one-step 4-electron pathway or two-step 4-electron pathway through H_2O_2 intermediate. The low efficiency for a catalyst towards ORR is often attributed to the latter and is also considered to be responsible for degradation of polymer electrolyte membrane. Au is not an active catalyst for direct di-oxygen reduction to H_2O as ORR on Au surface proceeds through two-step 4-electron pathway with hydrogen peroxide as the intermediate but for Au (100) plane and its vicinal surfaces in alkaline solutions (Adzic 1998). Pt reduces oxygen to water either through a 2-electron or a 4-electron process (Paulus et al 2001). Amelioration of ORR on Pt surfaces in presence of Au has been reported recently (Elhsissen et al 1999; Devarajan et al 2005; Luo et al 2005; Njoki et al 2005; Qian et al 2006; Hernandez-Fernandez et al 2008; Wang et al 2008, 2009; Liu et al 2009a, b; Ma et al 2010). However, the Au used in these studies is either used as a matrix to disperse the Pt sites or not as alloy particles.

Generally, LSV technique allows the determination of electrode-kinetic parameters for ORR (Paulus et al 2001). The ORR data obtained for the S-2(3:1) catalyst and S-4 at varying rotations, viz. 400, 800, 1200, 1600, 2000 and 2400 rpm. Both the catalysts show the current densities (current normalized to the geometric area of the electrode) to be proportional to rotation speed (ω). The number of electrons (n) is generally calculated from the slope of Levich plots using the equation

$$i_d = 0.62 n F A C D^{2/3} \gamma^{-1/6} \omega^{1/2}. \quad (1)$$

In short (1) can be expressed as:

$$i_d = B \omega^{1/2}, \quad (2)$$

where $B = 0.62 n F A C D^{2/3} \gamma^{-1/6}$ which is Levich slope, F is faraday constant, A the surface area of electrode, C the bulk concentration of oxygen in the electrolyte, D the diffusion coefficient of the reactant in electrolyte, γ the kinematic viscosity of solution and ω the angular frequency of rotation. Generally, under the mass-transfer-limiting condition, the Levich slope is constant. However, in the present study, when cathodic limiting current-densities are plotted vs $\omega^{1/2}$ a slightly curved line is observed. Hence, the inverse Levich plot, i.e. i^{-1} vs $\omega^{-1/2}$, is used to obtain the kinetic parameters, which is generally referred to as Koutecky–Levich (K–L) expression and is a straight line with non-zero intercepts.

Goaguen et al (1998) and Gojkovic et al (1998) have demonstrated a strong diffusion-resistance while using Nafion film over the catalyst layer in Koutecky–Levich type

analysis of the ORR currents. Since, their preparation method results in a relatively thick catalyst-layer (1–7 μm) with a high Nafion® content, film diffusion resistance plays an important role. By contrast, in the present study, the Nafion® ionomer is dispersed in the catalyst ink and thin layer of catalyst is deposited on substrate electrode (Paulus et al 2001). It is established that Nafion film diffusion resistance is negligible within the accessible current-density range up to 3600 rpm for the film thickness $<0.2 \mu\text{m}$. Accordingly, the kinetic current-densities can be extracted directly using the unmodified mass-transport correlation, viz. K–L equation, as follows:

$$\begin{aligned} 1/i &= 1/i_k + 1/i_d, \\ 1/i &= 1/i_k + 1/(B\omega^{1/2}). \end{aligned} \quad (3)$$

In (3), i_k (kinetic current) represents the current in the absence of any mass-transfer effects i.e. the current that would flow under the kinetic limitation if the mass transfers are efficient enough to keep the concentration at the electrode surface equal to the bulk value, regardless of the electrode reaction. Clearly, $i/\omega^{1/2}$ is constant only when i_k is very large. Otherwise, a plot of i vs $\omega^{1/2}$ will not be a straight line and would tend toward the limit $i = i_k$ as $\omega^{1/2} \rightarrow \infty$. But, a plot of $1/i$ vs $1/\omega^{1/2}$ should be linear and can be extrapolated to $\omega^{-1/2} = 0$ to yield $1/i_k$. Figure 9 represents the inverse current density (i^{-1}) as a function of the inverse of the square root of the rotation rate ($\omega^{-1/2}$), i.e. the so-called K–L plot. The linearity and the parallel character of these plots are suggestive of first-order kinetics with respect to molecular oxygen. From the K–L plots, S-2(3:1) catalyst shows enhanced kinetic current-density (i_k) in relation to Pt/C (S-4), which clearly indicates that the incorporation of Au into Pt matrix improves ORR.

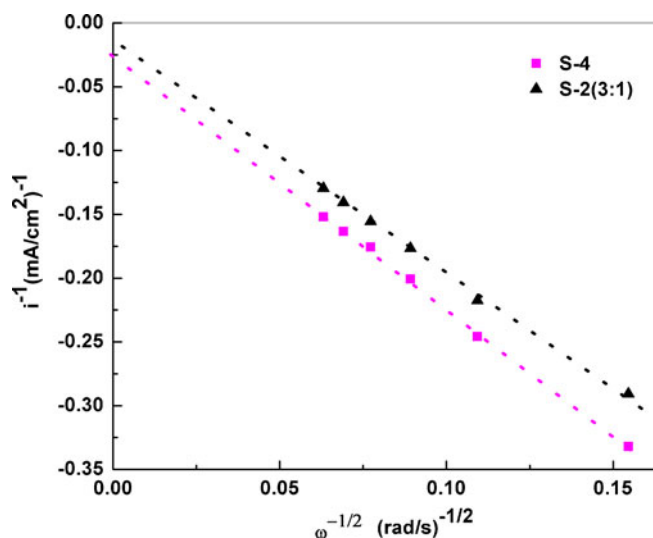


Figure 9. Levich–Koutecky plots for S-2 (3:1) and S-4 catalysts at 0.46 V vs SCE.

In general, the efficiency of catalyst can be obtained from the value of n during ORR. The actual number of electrons transferred by each oxygen molecule is calculated from the following values: (i) diffusion coefficient of $O_2(D)$ as $1.93 \times 10^{-5} \text{ cm}^2 \text{ s}^{-1}$ (Markovic *et al* 1999), (ii) kinematic viscosity of the solution (γ) as $1.009 \times 10^{-2} \text{ cm}^2/\text{s}$ (Markovic *et al* 1999) and (iii) concentration of dissolved O_2 in solution (C) as $1.26 \times 10^{-3} \text{ mol L}^{-1}$ (Lide 1995). From the slope of K–L plot (B), the value of n is calculated to be 4 for the S-2(3:1) catalyst. These values are higher than that for S-4 system. The S-2 catalyst reported here promotes the one step 4-electron transfer ORR. Furthermore, the ring current for Pt–Au catalyst shows negligible generation of hydrogen peroxide akin to that reported by Zhang *et al* (2007) suggesting a four-electron reduction of oxygen to water. As the S-2 catalysts reported here promote the 4-electron-ORR through one step reduction of di-oxygen to water without generation of peroxide, higher durability is also anticipated for the membrane electrolyte.

4. Conclusions

Carbon-supported Pt–Au alloy is prepared by three different methods, viz. colloidal, impregnation and micro-emulsion. Pt–Au catalysts prepared through colloidal and micro-emulsion methods result in homogenous solid solutions, while the catalyst prepared by impregnation method results in segregated Pt and Au particles. Among the three methods of preparation of Pt–Au catalyst, the catalyst prepared by colloidal method is found to perform better towards ORR in relation to the catalyst impregnation and micro-emulsion. Among the various Pt–Au/C catalysts prepared by colloidal method with varying atomic ratios of Pt to Au, S-2(3:1) i.e. Pt–Au (3:1)/C, shows maximum electrochemical activity towards ORR.

Acknowledgements

Financial support from CSIR, New Delhi, through a supra-institutional project under EFYP is gratefully acknowledged.

References

- Adzic R R 1998 in *Electrocatalysis* (eds) J Lipkowski and P N Ross (New York: Wiley-VCH) p. 197
- Antolini E, Salgado J R C and Gonzalez E R 2005 *J. Electroanal. Chem.* **580** 145
- Berg C, Venvik H J, Strisland F, Ramstad A and Borg A 1998 *Surf. Sci.* **409** 1
- Bockris J O M and Srinivasan S 1969 *Fuel cells: Their electrochemistry* (USA: McGraw-Hill Book Company)
- Bond G C 2007 *Platinum Metals Rev.* **51** 63
- Devarajan S, Bera P and Sampath S 2005 *J. Colloid Interf. Sci.* **290** 117
- El-Deab M S and Osaka T 2002a *Electrochem. Commun.* **4** 288
- El-Deab M S and Osaka T 2002b *Electrochim. Acta* **47** 4255
- El-Deab M S and Osaka T 2003 *J. Electroanal. Chem.* **553** 107
- Elhissen K T, Bonet F, Silvert P Y and Urbina R H 1999 *J. Alloys Compd* **292** 96
- Fernandez J L, Raguveer V, Manthiram A and Bard A J 2005 *J. Am. Chem. Soc.* **127** 13100
- Gasteiger H A, Kocha S S, Sompalli B and Wagner F T 2005 *Appl. Catal. B. Environ.* **56** 9
- Gloaguen F, Convert P, Gamburzev S, Velev O A and Srinivasan S 1998 *Electrochim. Acta* **43** 3767
- Gojkovic S L, Zecevic S K and Savinell R F 1998 *J. Electrochem. Soc.* **145** 3713
- Gong Y, Yeboah Y D, Lvov S N, Balashov V and Wang Z 2007 *J. Electrochem. Soc.* **154** B560
- Goodenough J B, Manoharan R, Shukla A K and Ramesh K V 1989 *Chem. Mater.* **1** 391
- Gottesfeld S and Zawodzinski T A 1997 in *Advances in electrochemical science and engineering* (eds) R C Alkire *et al* (Weinheim: Wiley-VCH), Ch. 4, **Vol. 5**
- Haruta M 1997 *Catal. Today* **36** 153
- Haruta M 2005 *Nature* **437** 1098
- Hernandez-Fernandez P, Rojas S, Ocon P, Gomez de la Fuente J L, San Fabian J, Sanza J, Pena M A, Garcia-Garcia F J, Terreros P and Fierro J L G 2007 *J. Phys. Chem.* **C111** 2913
- Hernandez-Fernandez P, Rojas S, Ocon P, de Frutos A, Figueroa J M, Terreros P, Pena M A and Fierro J L G 2008 *J. Power Sources* **177** 9
- Hughes M D *et al* 2005 *Nature* **437** 1132
- Janssens T V W, Carlsson A, Puig-Molina A and Clausen B S 2006 *J. Catal.* **240** 108
- Kristian N and Wang X 2008 *Electrochem. Commun.* **10** 12
- Li H, Xin Q, Li W, Zhou Z, Jiang L, Yang S and Sun G 2004 *Chem. Commun.* **25** 2776
- Lide D R 1995 *CRC handbook of chemistry and physics* (Boca Raton, FL: CRC Press) 75th ed.
- Lima F H B, Lizcano-Valbuena W H, Teixeira-Neto E, Nart F C, Gonzalez E R and Ticianelli E A 2006 *Electrochim. Acta* **52** 385
- Liu C W, Wei Y C and Wang K W 2009a *J. Colloid Interf. Sci.* **336** 654
- Liu C W, Wei Y C and Wang K W 2009b *Electrochem. Commun.* **11** 1362
- Lopez N and Norskov J K 2002 *J. Am. Chem. Soc.* **124** 11262
- Luo J *et al* 2005 *Catal. Today* **99** 291
- Luo J, Njoki P N, Lin Y, Wang L and Zhong C J 2006 *Electrochem. Commun.* **8** 581
- Ma Y, Zhang H, Zhong H, Xu T, Jin H and Geng X 2010 *Catal. Commun.* **11** 434
- Markovic N M, Gasteiger H A, Grgur B N and Ross P N 1999 *J. Electroanal. Chem.* **467** 157
- Mathiyarasu J and Phani K L N 2007 *J. Electrochem. Soc.* **154** B1100
- Mott D, Luo J, Njoki P N, Lin Y, Wang L and Zhong C J 2007 *Catal. Today* **122** 378
- Njoki P N, Luo J, Wang L, Maye M M, Quiazar H and Zhong C J 2005 *Langmuir* **21** 1623
- Paulus U A, Schmidt T J, Gasteiger H A and Behm R J 2001 *J. Electroanal. Chem.* **495** 134
- Pourbaix M 1974 *Atlas of electrochemical equilibria in aqueous solutions* (USA: National Association of Corrosion Engineers)

- Qian L, Sha Y and Yang X 2006 *Thin Solid Films* **515** 1349
- Selvarani G, Vinod Selvaganesh S, Krishnamurthy S, Kiruthika G V M, Sridhar P, Pitchumani S and Shukla A K 2009a *J. Phys. Chem.* **C113** 7461
- Selvarani G, Maheswari S, Sridhar P, Pitchumani S and Shukla A K 2009b *J. Electrochem. Soc.* **156** B1354
- Shao M H, Huang T, Liu P, Zhang J, Sasaki K, Vukmirovic M B and Adzic R R 2006a *Langmuir* **22** 10409
- Shao M H, Sasaki K and Adzic R R 2006b *J. Am. Chem. Soc.* **128** 3526
- Wang J, Yin G, Wang G, Wang Z and Gao Y 2008 *Electrochem. Commun.* **10** 831
- Wang J, Yin G, Liu H, Li R, Flemming R L and Sun X 2009 *J. Power Sources* **194** 668
- Xu Y and Mavrikakis M 2003 *J. Phys. Chem.* **B107** 9298
- Yuan W, Scott K and Cheng H 2006 *J. Power Sources* **163** 323
- Zhang J, Sasaki K, Sutter E and Adzic R R 2007 *Science* **315** 220